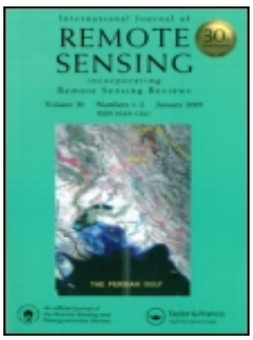

International Journal of Remote Sensing

ISSN: 0143-1161 (Print) 1366-5901 (Online) Journal homepage: http://www.tandfonline.com/loi/tres20

Land-use/land-cover change and its influence on surface temperature: a case study in Beijing City

Haiyong Ding & Wenzhong Shi

To cite this article: Haiyong Ding & Wenzhong Shi (2013) Land-use/land-cover change and its influence on surface temperature: a case study in Beijing City, International Journal of Remote Sensing, 34:15, 5503-5517, DOI: 10.1080/01431161.2013.792966

To link to this article: http://dx.doi.org/10.1080/01431161.2013.792966

International Journal of Remote Sensing, 2013
Vol. 34, No. 15, 5503–5517, http://dx.doi.org/10.1080/01431161.2013.792966

Land-use/land-cover change and its influence on surface temperature: a case study in Beijing City

Haiyong Ding[a] and Wenzhong Shi[b]*

[a]*School of Remote Sensing, Nanjing University of Information Science and Technology, Nanjing 210044, People's Republic of China;* [b]*Department of Land Surveying and Geo-informatics, The Hong Kong Polytechnic University, Hong Kong, People's Republic of China*

(*Received 19 October 2011; accepted 3 December 2012*)

Rapid global economic development has resulted in a corresponding intensification of urbanization, which has in turn impacted the ecology of vast regions of the world. A series of problems have thus been introduced, such as changes in land-use/land-cover (LULC) and changes in local climate. The process of urbanization predominantly represents changes in land-use, and is deemed by researchers to be the chief cause of climate change and ecological change. One of the principal purposes of the research in this field is to find ways to mitigate the influence of land-use change on local or global environments. In the study presented in this article, satellite images were utilized to extract information regarding land-use in Beijing City, and to develop maps of land surface temperature (LST) during two different periods of time: 2 August 1999 and 8 August 2010. A supervised classification scheme, a support vector machine, was used to derive the land-use change map for the above periods. Maps of surface temperature are derived from the thermal band of Landsat images using the mono-window algorithm. Results from post-classification comparison indicated that an increase in impervious surface areas was found to be dramatic, while the area of farmland decreased rapidly. The changes in LULC were found to have led to a variation in surface temperature, as well as a spatial distribution pattern of the urban heat island phenomenon. This research revealed that the hotspots were mainly located in areas dominated by three kinds of material: bare soil, rooftops, and marble surfaces. Results from the local Moran's I index indicated that the use of lower surface temperature materials will help to mitigate the influence of the urban heat island phenomenon. The results of this research study provide a reference for government departments involved in the process of designing residential regions. Such a reference should enable the development of areas sympathetic to environmental changes and hence mitigate the effects of the growing intensity of urbanization.

1. Introduction

Urbanization has become an inevitable worldwide trend, resulting from rapid global economic development and the corresponding increase in population. The latter is composed of the workers necessary to feed such expansion, as well as those eager to prosper from the potentially high living standards that economic development may bring. Agriculture and land-use change during the process of urbanization is recognized as the most important anthropogenic influence on climate change (Jones et al. 1990; Kalnay and Cai 2003; Owen,

*Corresponding author. Email: john.wz.shi@polyu.edu.hk

Carlson, and Gilies 1998). Kalnay and Cai (2003) concluded that half the observed decrease in diurnal temperature range was due to urban sprawl and land-use changes. In 1998, the land-cover index (LCI) was proposed by Owen, Carlson, and Gilies (1998) as a new approach to enable quantitative description of the climatic effect of urbanization, such as the urban heat island (UHI) effect. The function of this index is to enable the analysis of urban temperature changes, with specific reference to an analysis of the changes in land-use on a neighbourhood scale. Clear influences of urbanization on the landscape such as watersheds, riparian areas, wildlife habitat, and water supplies have been observed in European cities and several US cities (Alig, Kline, and Lichtenstein 2004; Antrop 2004; Buyantuyev, Wu, and Gries 2007; Rottenborn 1999). Rottenborn (1999) found that bird species richness and density decreased at a location when the number of bridges near that location increased and the volume of native vegetation also decreased. Dewan and Yamaguchi (2009) found that substantial growth of built-up areas in Greater Dhaka resulted in a significant decrease in the area of water bodies, cultivated land, vegetation, and wetlands. In addition, rapid urban expansion induced a wide range of environmental impacts, including habitat quality (Bayarsaikhan et al. 2009; Dewan and Yamaguchi 2009; Li and Zhao 2003).

Another significant effect of urbanization is seen as variation in surface temperature (Chen et al. 2006; Hamdi 2010), and in some cases has become known as the UHI. Typical characteristics of UHI surface temperature variation include simultaneous differences in air and land surface temperature (LST) from those in the surrounding rural regions (Hart and Sailor 2009; Hu and Jia 2010; Zhang and Wang 2008). Over the past 30 years, such phenomena have been extensively studied in America, Europe, and Asia (Imhoff et al. 2010; Lee and French 2009; Li et al. 2009; Memon, Leung, and Liu 2009; Streutker 2003). It has been found that changes in land-use/land-cover (LULC) influenced the composition of ground substances, such as major impacts on the evaporation of water and the process of energy exchange (Hung et al. 2006; Stathopoulou and Cartalis 2007; Umamaheshwaran and Weng 2009).

To analyse or quantify the effect of UHI, researchers have employed remotely sensed images such as Landsat Thematic Mapper/Enhanced Thematic Mapper Plus (TM/ETM+), Moderate Resolution Imaging Spectroradiometer (MODIS), Advanced Very High Resolution Radiometer (AVHRR), and Advanced Spaceborne Thermal Emission and Reflection (ASTER) data to obtain large-scale observations (Liu and Weng 2008; Nichol et al. 2009; Qian, Cui, and Chang 2006; Srivastava, Majumdar, and Bhattacharya 2009; Xiao and Weng 2007). AVHRR data were used by Streutker (2003) to analyse UHI characteristics in Houston, USA. To understand the impacts of urbanization, Hung et al. (2006), using remotely sensed images, analysed the effects of UHI in 18 major cities. Qian, Cui, and Chang (2006) utilized Landsat TM/ETM+ data and geographic information system (GIS) technologies to identify patterns of LULC and to quantify the relationship between LULC change and the variation of LST. They found that urban growth caused LST to rise by 4.56°C between 1990 and 2000.

The majority of the studies above revealed that LULC change had a predominant impact on local environments, in the form of local climate change, watershed alteration, and the degradation of forests. Although much attention had been paid to the relationship between LULC and LST, further studies are necessary to achieve greater extracted land surface parameter accuracy, and also to focus on the exploration of the relationships between LULC and LST change, in order to better understand the environmental influence of urbanization.

This research study aims to investigate the influence of urbanization on land-cover and the resulting overall changes caused by the ensuing urban expansion into rural or less urbanized areas. An example of an area of rapid economic and urban expansion is provided by

the city of Beijing, which is the focus of this research study. The speed and volume of development that has taken place in Beijing over the past 30 years is such that the UHI effect upon the region has become the focus of discussion and research studies for approximately the last 10 years. The results of these research studies form a foundation from which the present authors explore the relationship between urban LULC change and the pattern of LST at different times. Landsat TM/ETM+ images are used to derive data on LST and LULC change. The widespread post-classification comparison and image difference methods are used to extract LULC change information and to identify locations exhibiting temperature variation.

2. Study area, data, and methodologies

2.1. Study area and data

The study area, the city of Beijing, is located to the north of the North China Plain, and extends from 39° N to 41° N (latitude) and 115° E to 117° E (longitude) (Figure 1). The area covers 16,410 km^2. In recent years, Beijing has been ranked as one of the fastest-growing cities in China, both economically and in area. Its gross domestic product (GDP) increased from 217.45 billion ($\times 10^9$) Yuan in 1999 to 900 billion Yuan in 2007, and it is reported that in 2009 it reached 1.186 trillion ($\times 10^{12}$) Yuan. During the period 1999 to 2007, Beijing experienced a rapid population increase from 12.57 million in 1999 to 16.33 million in 2007. This rapid population increase and economic growth have resulted in the city's accelerated urbanization and, as such, provides a scenario for which monitoring and analysis, in terms of LULC, is worthwhile.

Landsat images have been extensively utilized for UHI study (Buyantuyev, Wu, and Gries 2007; Kato and Yamaguchi 2005; Li and Zhao 2003; Lu and Weng 2005; Sobrino, Jimenez-Munoz, and Paolini 2004; Srivastava, Majumdar, and Bhattacharya 2009). Landsat 5 provides TM images that have six bands in the visible and near infrared regions with 30 m spatial resolution, and one thermal infrared band with 120 m spatial resolution. Landsat 7 provides eight bands, i.e. six each in the visible and near infrared regions with 30 m spatial resolution, one thermal infrared band with 60 m spatial resolution and one panchromatic band with 15 m spatial resolution. Because of the higher spatial resolution of the thermal infrared band, Landsat images were chosen as a suitable medium for the investigation of LULC and LST change. Landsat TM/ETM+ images, dated 2 August 1999 and 8 August 2010, were used in this research as representatively reflecting quantitatively the change in LULC and LST.

2.2. Methodologies used

Since no cloud cover was noted during image acquisition, atmospheric corrections are not included. Spatial registration was conducted on the six spectral bands of both images acquired over two days: 2 August 1999 and 8 August 2010. About 20 control points were manually selected from typical features and unchanged structures such as road intersections. To avoid the detection of 'false' change, polynomial warp was executed by use of a residual error of less than 0.1 pixel.

2.2.1. Image classification and accuracy assessment

The LULC change resulting from the rapid expansion of the city over the past 10 years can be quantified by image classification and segmentation. As a non-parametric method and statistical learning theory, a support vector machine (SVM) can learn from a smaller

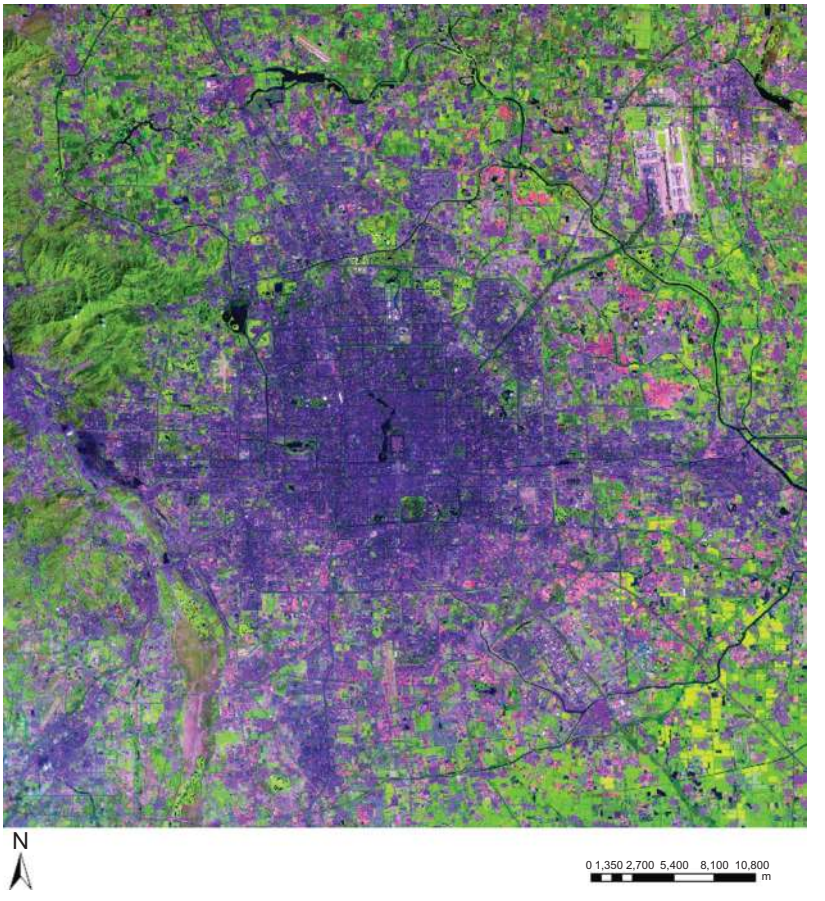

Figure 1. The study area, the city of Beijing (TM image, 8 August 2010).

number of training samples and has better pattern recognition capabilities. Therefore, the SVM classification model in Environment for Visualizing Images (ENVI) software was used in this research to extract the LULC information (Exelis Visual Information Solutions, Inc., Boulder, CO, USA). Six distinctive LULC types (i.e. trees, bare soil, water bodies, vegetation, built-up areas, and marble surfaces) were identified from the image acquired on 2 August 1999. The mountains located at west of Beijing were covered by trees which had the spectral characteristics of vegetation, and therefore this tree type was identified as an individual land-cover type. The urban regions were composed of roads covered with asphalt or concrete, buildings, and impervious surface areas. The marble surface at Beijing airport, specified as an impervious surface, had a particular spectral reflection on the satellite image. Seven land-use types were recognized from the TM data acquired on 8 August 2010. These included trees, vegetation, water bodies, bare soil, built-up areas, concrete surfaces, and rooftops. Different from other land-cover types, concrete surfaces were found to have a high albedo, and thus a single land-use type was defined and identified. Rooftops were considered as a single land-use type, thus accommodating a diversity of factories with huge rooftops covered by blue plastic material. A detailed description of LULC type is given in Table 1.

Assessment of classification accuracy is important in accurate quantification of change detection. Regions of interest, modelled using ENVI software, were used as reference data

Table 1. Land-use/land cover types for classification.

Land-use/land-cover types	Description
Trees	Mountain forest, farmland trees, roadside trees, trees around water bodies
Vegetation	Farmland, gardens
Water bodies	Rivers, lakes
Built-up	Roads, buildings, residential areas
Soil	Bare soil, farmland
Marble	Paved square
Rooftops	Manufactory roofs

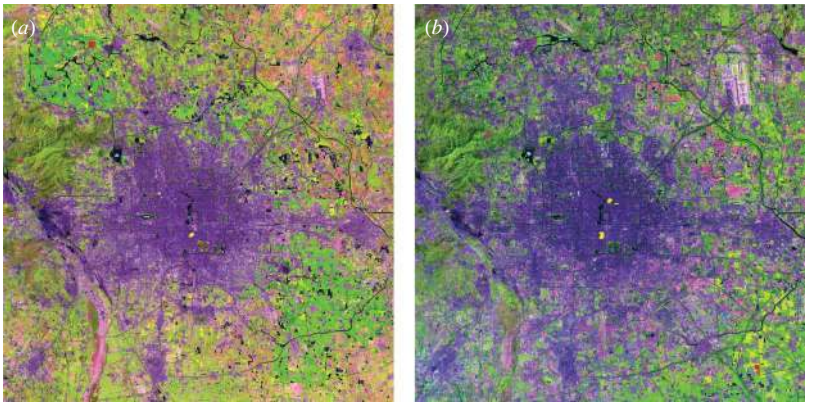

Figure 2. Distribution of samples of different classes for accuracy assessment. (*a*) 2 August 1999; (*b*) 8 August 2010. Colour coding: trees, maroon; vegetation, red; water, cyan; soil, blue; built-up, yellow; marble, magenta; rooftops, green.

for different LULC types. A total of 10,334 point samples were randomly selected for the ETM+ data from 2 August 1999, and a total of 12,796 point samples were randomly selected for the TM data from 8 August 2010 (Figure 2). QuickBird and Ikonos images acquired during 2006, 2007, and 2008 were used to verify the reference point samples for some parts of the study area. Google Earth was used to identify the rooftop type and to help in extraction of ground truth samples.

Confusion matrices for different image data were created using the test samples to check the accuracy of the classification results, as shown in Tables 2 and 3. It will be seen in the tables that the overall accuracy for 1999 and 2010 was 94.62% and 97.08%, respectively, and the Kappa coefficients for corresponding maps were 0.9325 and 0.965, respectively. LULC change data could be deduced from these data, which were qualified by further analysis.

LULC changes occurring over the previous 10 years were detected using a post-classification comparison method, which has been extensively utilized to demonstrate the LULC change process. The accuracy of classification results and post-classification method enabled the development of a cross-matrix to describe change types within the study area.

2.2.2. Retrieval of land surface temperature

The LST was retrieved by utilization of thermal infrared band (10.4–12.5 μm) data from TM/ETM+. The extraction of the temperature data from the high-gain band was used as it had a less striped texture and a wider range of recorded digital number (DN) values. First,

Table 2. Confusion matrices of pre-image LULC classification, 2 August 1999.

	Reference data					
	Trees	Vegetation	Water	Soil	Built-up	Marble
Trees	2323	450	0	0	0	0
Vegetation	0	1878	0	0	0	0
Water	0	0	978	0	0	0
Soil	0	58	0	2206	5	1
Built-up	0	0	0	0	2342	0
Marble	0	0	0	51	0	259
Total	2323	2386	978	2257	2350	260
Producer's accuracy (%)	100	78.71	100	97.74	99.66	99.62

Table 3. Confusion matrices of post-image LULC classification, 8 August 2010.

	Reference data						
	Trees	Vegetation	Water	Soil	Built-up	Marble	Rooftops
Trees	1483	237	0	0	0	0	0
Vegetation	241	1998	0	0	0	0	0
Water	0	0	1114	0	0	0	0
Soil	0	0	0	563	0	7	0
Built-up	0	0	0	0	1621	0	6
Marble	0	0	0	0	4	771	3
Rooftops	0	0	0	0	0	0	999
Total	1724	2235	1114	563	1625	778	1008
Producer's accuracy (%)	100	89.40	100	100	99.75	99.10	99.11

the DN values were converted to the top-of-atmosphere (TOA) radiance measured by an instrument using the following equation (1):

$$L_\lambda = \frac{L_{\max} - L_{\min}}{(\mathrm{QCAL})_{\max} - (\mathrm{QCAL})_{\min}}((\mathrm{DN}) - (\mathrm{QCAL})_{\min}) + L_{\min}, \quad (1)$$

where λ is wavelength; L_λ is the TOA radiance at the sensor's aperture in W m^{-2} sr^{-1} μm^{-1} and $\mathrm{QCAL}_{\max}$ and $\mathrm{QCAL}_{\min}$ are the highest and the lowest points of the range of rescaled radiance in DN, with values 255 and 0, respectively. $L_{\min}$ and $L_{\max}$ are the TOA radiances that are scaled to $\mathrm{QCAL}_{\min}$ and $\mathrm{QCAL}_{\max}$ in W m^{-2} sr^{-1} μm^{-1} and can be found in the Landsat 7 Science Data Users Handbook (http://landsathandbook.gsfc.nasa.gov/pdfs/Landsat7_Handbook.pdf).

The spectral radiance L_λ should be further converted to the at-sensor brightness temperature BT in kelvin and the conversion equation can be written as

$$\mathrm{BT} = \frac{K_2}{\ln\left(\frac{K_1}{L_\lambda}\right) + 1}, \quad (2)$$

where BT is the at-sensor brightness temperature in kelvin; K_1 (1282.71 K) and K_2 (666.09 Wm^{-2} sr^{-1} μm^{-1}) are calibration constants. Brightness temperature is that obtained by a blackbody to produce the same radiance at the same wavelength. This means

that the brightness temperature cannot reflect the 'real' LST because of the various emissions from different land-cover types. Hence, the brightness temperature must be converted to the LST using the following formula:

$$\mathrm{LST} = \frac{(\mathrm{BT})}{1 + \frac{\lambda(\mathrm{BT})}{\rho} \ln \varepsilon}, \tag{3}$$

where LST is the LST in kelvin, BT is the at-sensor brightness temperature in kelvin, λ (11.5 μm) is the wavelength of emitted radiance: $\rho = \mathrm{h} \times \mathrm{c}/\sigma = 1.438 \times 10^{-2}$ mK, σ is the Stefan–Boltzmann constant, h is Planck's constant, c is the velocity of light, and ε is the land surface emissivity (LSE).

LSE is a key parameter in the measurement of LST. It is difficult, however, to retrieve LSE directly from remotely sensed images. An optimization method was proposed to estimate LSE and LST simultaneously (Liang 2001), but this requires multiple thermal bands of which there is a shortage for Landsat images. Another method to estimate emissivity is to use the classification results. Each land-cover type realized from the classification results is allocated the corresponding emissivity. Classification errors and mixed pixels, however, introduce further severe emissivity error. In other studies reported in the literature, the relationship between emissivity and normalized difference vegetation index (NDVI) was found by means of empirical approaches. When NDVI < 0.2, the pixels are considered to be revealing bare soil and emissivity is assumed to be 0.97. When NDVI > 0.5, the pixels are considered to be revealing a fully vegetated area and a constant value for the emissivity is assumed to be 0.99. When $0.2 \leq \mathrm{NDVI} \leq 0.5$, the pixel is composed of a mixture of bare soil and vegetation, and emissivity is calculated according to the following equation:

$$\varepsilon_{\mathrm{TM6}} = 0.004 \cdot P_v + 0.986, \tag{4}$$

where $\varepsilon_{\mathrm{TM6}}$ is surface emissivity and P_v is the vegetation proportion obtained according to Sobrino, Jimenez-Munoz, and Paolini (2004):

$$P_v = \left[\frac{(\mathrm{NDVI}) - (\mathrm{NDVI})_{\min}}{(\mathrm{NDVI})_{\max} - (\mathrm{NDVI})_{\min}} \right]^2, \tag{5}$$

where $\mathrm{NDVI}_{\max} = 0.5$ is the threshold to separate the bare soil pixel and the mixed pixels; and $\mathrm{NDVI}_{\min} = 0.2$ is the threshold to separate the full vegetation pixel and the mixed pixels. NDVI can be expressed using the following equation:

$$\mathrm{NDVI} = \frac{\rho(\mathrm{band4}) - \rho(\mathrm{band3})}{\rho(\mathrm{band4}) + \rho(\mathrm{band3})}, \tag{6}$$

where ρ(band4) and ρ(band3) are the spectral reflectances of bands 4 and 3, respectively, for Landsat images. The parameters used to convert DN to spectral reflectance can be found in the metadata file associated with Landsat images.

2.2.3. *Local pattern of LST*

As spatial data, LST variation depends on the LULC distribution pattern (i.e. LST exhibits spatial dependency). Spatial dependency refers to those objects closely positioned in space, which tend to be more alike than objects that are further apart. Spatial similarity is usually expressed using autocorrelation of one variable. Moran's I index, which measures spatial autocorrelation in a signal among nearby locations in space, has been extensively utilized

to analyse the global level of autocorrelation by setting a series of lag distances. The local Moran's I, however, is more appropriate for assessing the autocorrelation character in the local region. The clustering of similar values in the local region can be represented using the positive value of Moran's I, while its negative value explains the clustering of dissimilar values; a value of zero indicates zero spatial autocorrelation. Due to the fact that the LST of surface materials is closely related to its composition, LST spatial distribution in the local region is closely associated with the shape of the materials, such as the strip-type of the road, the rectangle-type of squares and rooftops, and irregular shape of bare soil cover types. Therefore, in this research, using a 3 pixel × 3 pixel moving window with Queen's case contiguity, in which case eight neighbouring pixels all have been selected, the local Moran's I index was calculated to quantify the autocorrelation of LST in the local region.

3. Results and discussion

3.1. LULC change analysis

Spatial patterns of LULC in the study area for 1999 and 2010 are shown in Figure 3. In 1999, built-up, vegetation and soil were the dominant land-use types, with percentages of 25.77%, 25.75%, and 25.52%, respectively. It was found that there were dense built-up surfaces in the urban area, which were surrounded by farmland and mountains. Using the ring road constructed in recent years, land-use types were clearly separated one from each other. In this way, the urban area was mainly confined within the fourth ring road, the suburban region was mainly located between the fourth and fifth ring roads and the rural region was located outside the fifth ring road.

In 2010, built-up surface areas were the dominant land-use type with a percentage of 50.87, followed by tree groupings and vegetation (24.81% and 14.86%, respectively). The urban area was bounded by the fifth ring road, and the suburban region was located between the fifth and sixth ring roads. Many factory areas found in the classification map provided evidence of the development of the economy, while the emergence of factory rooftop types illustrated the decrease in farmland area.

The statistical post-classification comparison results are shown in Table 4. This comparison demonstrates the significant increase in the area of built-up surfaces; for example, about 52.45% of soil area and 34.25% of vegetation area in 1999 have been converted to built-up surfaces. The most notable change occurred in the LULC type 'soil', of which about 97.08% had changed to other land-use types, such as built-up, trees, vegetation, and rooftops. Another evident land-use change was found in the marble type, of which about 64.28% and 10.56% had been converted to built-up and rooftop areas, respectively. About 74.02% of the vegetation area had changed, with 34.25% and 6.16% becoming built-up and rooftop, respectively. In summary, over the past 10 years, significant increases in built-up surface area and a decrease in farmland surface had taken place.

3.2. Spatial and temporal characteristics of LST variation

3.2.1. Spatial and temporal distribution of LST pattern

Descriptive LST statistics for the study area were calculated, and are shown in Table 5. In 1999, LST ranged from 21.33°C to 44.96°C (mean, 28.83°C), while the corresponding figures for 2010 were 17.47–44.01°C (mean, 29.39°C). The mean LST of these two time points demonstrates that 8 August 2010 was a little warmer than 2 August 1999.

The LST maps for these dates are shown in Figure 4 to demonstrate the LST spatial distribution pattern. Several characters will be observed on the LST map for 1999. First,

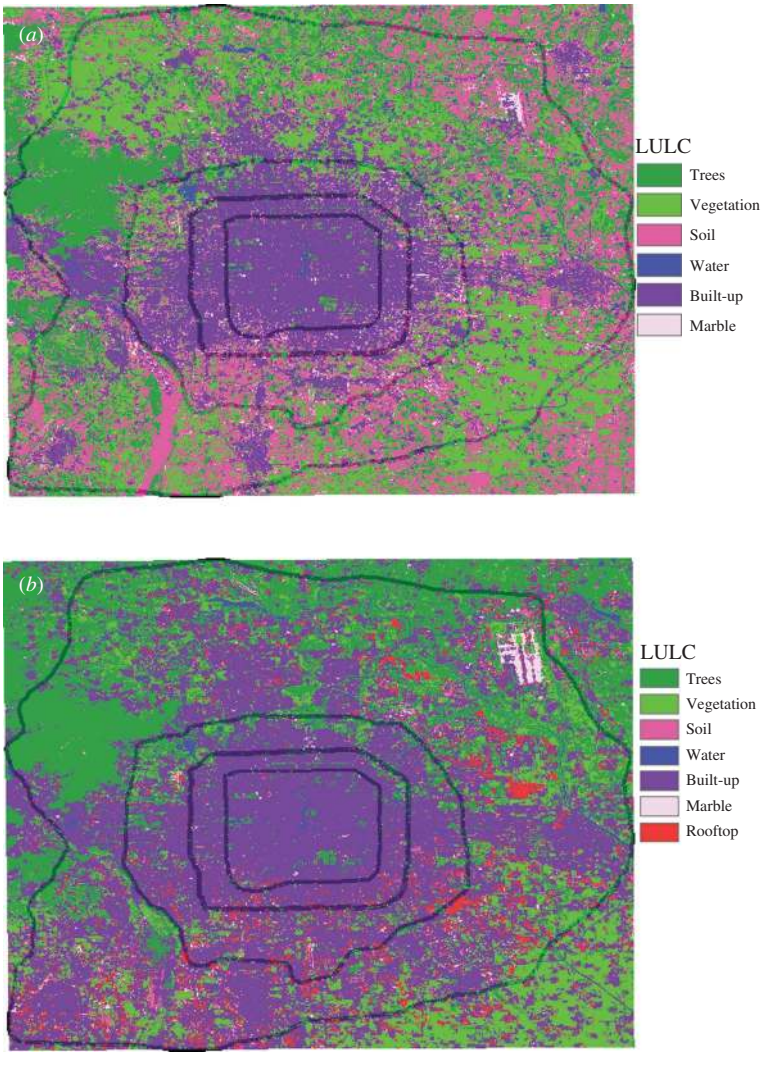

Figure 3. LULC maps of study area. (*a*) 2 August 1999; (*b*) 8 August 2010.

Table 4. Change detection statistics for LULC (%).

	2 August 1999			
8 August 2010	Trees	Vegetation	Water	Built-up
Trees	53.67	29.95	13.86	5.44
Vegetation	15.18	25.98	12.51	2.76
Water	0.50	0.79	37.82	0.67
Built-up	24.64	34.25	29.24	86.04
Marble	0.76	0.92	0.66	0.65
Soil	1.52	1.96	1.09	1.19
Rooftop	3.73	6.16	4.81	3.25
Class changes	46.33	74.02	62.18	13.96

Table 5. Descriptive statistics of LST for different time points.

	Minimum	Maximum	Mean	Standa
2 August 1999 (°C)	21.33	44.96	28.83	
8 August 2010 (°C)	17.47	44.01	29.30	

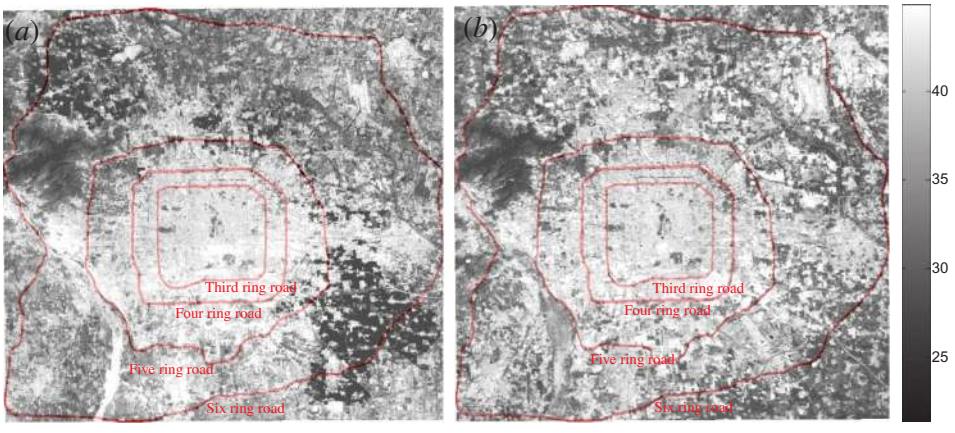

Figure 4. LST for 2 August 1999 (*a*) and 8 August 2010 (*b*).

there was a clear temperature gradient between the urban and rural areas due to the fact that the urban area surface was composed of roads and buildings covered with materials such as asphalt and concrete, all of which have a higher radiant temperature. Second, hotspots were mainly located in three land-use types: built-up, bare soil, and marble surfaces.

According to the LST map for 2010, the expansion of high-LST surfaces was significant in comparison with the 1999 map. It appears that these high-temperature surfaces were closely associated with impervious surfaces such as built-up, marble, and rooftop areas. The rural region of 1999 had become the suburban area of 2010, to accommodate the expansion of the city. The LST map indicates that the higher-LST areas were bounded by the fifth ring road and between the fifth and sixth ring roads, and that the low-LST area was located outside the sixth ring road. Three types of hotspot location were identified in 2010: Beijing International Airport, factory rooftops, and bare soils.

3.2.2. Local autocorrelation of LST

The local measure of Moran's I was calculated using ENVI software, and the maps are shown in Figure 5. For 1999, the value of global Moran's I was 0.9683, which indicates that there was positive autocorrelation among LST when the lag distance was one pixel. In the left-hand map, the value of local Moran's I ranged between –0.2539 and 23.53, and its average of 0.8582 indicates that most locations had an LST value similar to that of their eight neighbours. Soil, trees, and vegetation had higher Moran's I due to weak spatial heterogeneity, while this value was lower in built-up locations in the urban area since there was a significant mixture of materials such as trees, buildings, and roads.

In 2010, the value of global Moran's I was 0.9652, which was similar to that in 1999, while the range of local Moran's I found was between –0.1825 and 47.33 (average, 1.29). Higher values of Moran's I appeared in locations characterized by single building materials such as airport and rooftop surfaces. Unlike trees and vegetation types, the pixel and its

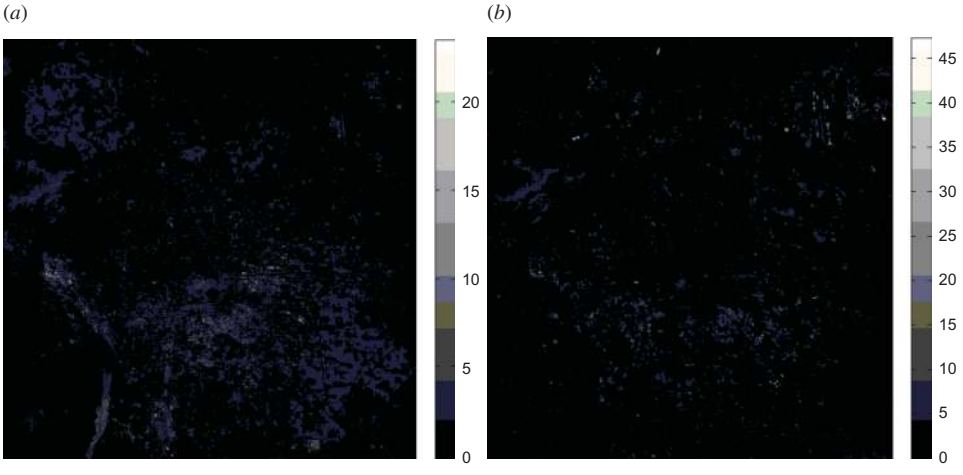

Figure 5. Maps of local Moran's I index using LST data: 2 August 1999 (*a*) and 8 August 2010 (*b*).

neighbouring pixels among these land surface types had almost the same radiant temperature, thus inducing higher autocorrelation. Trees and rooftops had a high Moran's I index in 2010, consistent with that in 1999. Although average Moran's I was higher in 2010, values were smaller in most sites as a result of urban expansion.

3.3. Relationship between LST and LULC

Data from the literature in regard to the UHI phenomenon prove that LST is closely associated with the land-cover composition of materials, such as vegetation, forest, and soil. Therefore, it was found necessary to explore the relationship between LST and LULC to gain an insight into the establishment of UHI during the process of urbanization. Average LST and standard deviation (Std) associated with different land-cover types are shown in Table 6. In 1999, the maximum average LST was found in built-up areas, followed by marble and bare soil surfaces. The three LULC types trees, vegetation, and water had a lower LST compared with built-up areas. In 2010, similar to the results of 1999, four LULC types: rooftop, marble, soil, and built-up areas, had an average LST over 30°C, while the remaining three types had a lower LST. Rooftop surfaces converted from other LULC types such as soil, vegetation, and marble surfaces had the maximum average LST. This indicates that the process of urbanization induced an increase in LST when land-cover type changed from pervious to impervious materials, which have a higher radiant temperature. Further, air temperature increased during the complicated energy exchange process.

To analyse the influence of LULC change on LST change, the image difference method was used for LST maps to derive a temperature difference map (Figure 6). Six classes of temperature change were extracted according to the relationship between differences in LST, mean value (Mean), and Std of the LST difference image. For example, class 2 was identified as those pixels located at the interval (Mean + Std, Mean + 2 × Std) and the

Table 6. Mean LST of different land-cover types (mean value plus/minus standard deviation).

	Trees	Vegetation	Soil	Water	Built-up
1999 (°C)	26.85 ± 1.50	25.92 ± 1.63	30.13 ± 2.01	27.80 ± 2.25	31.77 ± 1.93
2010 (°C)	27.21 ± 1.30	26.90 ± 1.07	31.35 ± 1.88	27.94 ± 1.79	30.70 ± 1.78

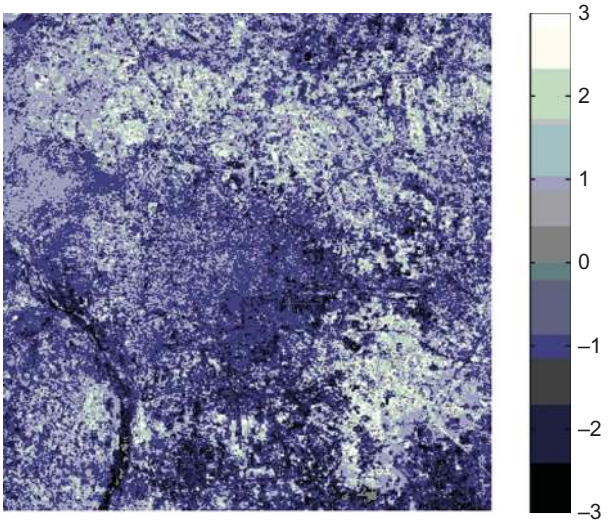

Figure 6. Temperature change maps derived by image difference method.

pixel labelled as class 1 located at the interval (Mean – Std, Mean). The temperature change gradient was clearly observed and most of the urban areas were classified as class 1, which means that the LST on 8 August 2010 was lower than that on 2 August 1999. The reason for this may be the increase in vegetation cover in the urban area, which can be seen in Table 4. LST increased quickly, due to most farmland in the rural area being converted to built-up and factory areas. LST was then classified as classes 2 and 3, as shown in Figure 6. However, because the soil type in the southwest of Beijing City had changed to other land-cover types such as vegetation or trees, these areas were classified as class 3, indicating decreased LST due to the change of land-use.

Samples for different LULC types were taken from the images to demonstrate the temperature difference when the land-use type changed (Table 7). It was noted that when previous land-cover types became a type with an impervious surface, such as that created by built-up, rooftop, and marble cover types, there was a clear increase in LST. The average LST decreased by about 8.64°C when soil was converted to vegetation cover type.

4. Driving force

4.1. Driving force from economic growth

Economic growth over the past 10 years has been the prominent driving force behind the urbanization of Beijing City. Data from the National Bureau of Statistics of China reveal that GDP in 2010 was 1.37779 trillion Yuan, while in 1999 it was 217.45 billion Yuan, showing a significant increase in economic income.

Table 7. Temperature change according to change in LULC type, 1999–2010.

	Veg. → Built-up	Veg. → Rooftops	Veg. → Marble
Temp. diff (°C)	8.02 ± 1.30	9.52 ± 1.03	7.72 ± 0.83

4.2. Driving force from population growth

Population growth has been the second driving force behind the expansion of Beijing. Statistical data from the National Bureau of Statistics of China show that the population of Beijing City rose from 12.57 million in 1999 to 19.61 million in 2010. This increase in population naturally necessitated the provision of more houses, jobs, and public places. Lack of the latter would be likely to seriously disturb economic development due to social unrest.

4.3. Driving force from other factors

Further forces associated with those mentioned above drove the sprawl of Beijing City. The first was the need to improve the living and working environment, and the second was the need to improve traffic conditions. The network of expressways and highways in 2009 showed a marked increase over that in 1999 (Table 8). These two factors pressured the government to formulate better plans for expansion of the city.

5. Conclusions

LULC change during the process of urban expansion of Beijing City had typical influences on local climate spatial patterns, as evidenced by the UHI phenomenon. To assess LULC change and its impact on LST in the city, remote sensing images from Landsat satellites were utilized to obtain maps of land-cover classification and LST. Several conclusions can be drawn from this research. First, a significant change in LULC took place in this area over the 10 years of the study. This change is seen in the increase in impervious surface areas such as built-up areas, marble surfaces, and rooftop areas, and the decrease in areas of vegetation. Second, it is apparent that LULC change is the predominant factor in LST variation found to be closely associated with the physical characteristics of construction materials used. Bare soil, rooftops, and marble surfaces have been demonstrated to have a higher surface temperature compared with that of other forms of land-cover, such as water and vegetation. Temperature variation can be identified when one type of land-cover is converted to another. Third, the autocorrelation of LST calculated from local Moran's I revealed that a stronger heterogeneous nature of surface composition leads to smaller values of local Moran's I. Hence, during the process of the design of residential areas, ideally the use of materials emitting lower surface temperatures is advisable to mitigate the influence of UHI.

Research studies, using remote sensing images for UHI and LULC changes, indicated that remotely sensed images have the ability to demonstrate changes in land-use and variation in surface temperature. Compared with methods using data from ground-based meteorological stations, remote sensing provides higher spatial resolution information about land-cover change and temperature variation. However, the remote-sensing method is limited by (1) the effect of cloud cover, which negatively affects imaging quality, and (2) the restricted revisiting cycle of the satellite for the individual location. To alleviate

Table 8. Length of highways in Beijing City, 1999 and 2009 (km).

	Expressway	Highway class I	Highway class II	Highway below class IV	Total length of highways
1999	190	247	1083	460	12,498
2009	884	914	3106	204	20,755

these limitations, future work should focus on the integrated application of multi-sensor satellite data and meteorological data from ground-based stations to provide more accurate land-cover change information.

Acknowledgements

This research was supported by the research project 'Remote sensing for the promotion of sustainable urbanization' (1-ZV4V) from the Department of Land Surveying and Geo-Informatics, The Hong Kong Polytechnic University. The project was sponsored by the Scientific Research Foundation of Key Laboratory for Land Environment and Disaster Monitoring of SBSM (Grant No. LEDM2010B06) and the research fund of NUIST (Grant No. 20090207). The authors would like to thank the anonymous reviewers for their valuable comments on this article.

References

Alig, R. J., J. D. Kline, and M. Lichtenstein. 2004. "Urbanization on the US Landscape: Looking Ahead in the 21st Century." *Landscape and Urban Planning* 69: 219–234.

Antrop, M. 2004. "Landscape Change and the Urbanization Process in Europe." *Landscape and Urban Planning* 67: 9–26.

Bayarsaikhan, U., B. Boldgiv, K. Kim, K. Park, and D. Lee. 2009. "Change Detection and Classification of Land Cover at Hustai National Park in Mongolia." *International Journal of Applied Earth Observation and Geoinformation* 11: 273–280.

Buyantuyev, A., J. Wu, and C. Gries. 2007. "Estimating Vegetation Cover in an Urban Environment Based on Landsat ETM+ Imagery: A Case Study in Phoenix, USA." *International Journal of Remote Sensing* 28: 269–291.

Chen, X., H. Zhao, P. Li, and Z. Yin. 2006. "Remote Sensing Image-Based Analysis of the Relationship Between Urban Heat Island and Land Use/Cover Changes." *Remote Sensing of Environment* 104: 133–146.

Dewan, A. M., and Y. Yamaguchi. 2009. "Land Use and Land Cover Change in Greater Dhaka, Bangladesh: Using Remote Sensing to Promote Sustainable Urbanization." *Applied Geography* 29: 390–401.

Hamdi, R. 2010. "Estimating Urban Heat Island Effects on the Temperature Series of Uccle (Brussels, Belgium) Using Remote Sensing Data and a Land Surface Scheme." *Remote Sensing* 2: 2773–2784.

Hart, M. A., and D. J. Sailor. 2009. "Quantifying the Influence of Land-Use and Surface Characteristics on Spatial Variability in the Urban Heat Island." *Theoretical and Applied Climatology* 95: 397–406.

Hu, Y., and G. Jia. 2010. "Influence of Land-Use Change on Urban Heat Island Derived from Multi-Sensor Data." *International Journal of Climatology* 30: 1382–1395.

Hung, T., D. Uchihama, S. Ochi, and Y. Yasuoka. 2006. "Assessment with Satellite Data of the Urban Heat Island Effects in Asian Mega Cities." *International Journal of Applied Earth Observation and Geoinformation* 8: 34–48.

Imhoff, M. L., P. Zhang, R. E. Wolfe, and L. Bounoua. 2010. "Remote Sensing of the Urban Heat Island Effect Across Biomes in the Continental USA." *Remote Sensing of Environment* 114: 504–513.

Jones, P. D., P. Y. Groisman, M. Coughlan, N. Plummer, W.-C. Wang, and T. R. Karl. 1990. "Assessment of Urbanization Effects in Time Series of Surface Air Temperature Over Land." *Nature* 347: 169–172.

Kalnay, E., and M. Cai. 2003. "Impact of Urbanization and Land-Use Change on Climate." *Nature* 423: 528–532.

Kato, S., and Y. Yamaguchi. 2005. "Analysis of Urban Heat-Island Effect Using ASTER and ETM+ Data: Separation of Anthropogenic Heat Discharge and Natural Heat Radiation from Sensible Heat Flux." *Remote Sensing of Environment* 99: 44–54.

Lee, S., and S. P. French. 2009. "Regional Impervious Surface Estimation: An Urban Heat Island Application." *Journal of Environmental Planning and Management* 52: 477–496.

Li, J., X. Wang, X. Wang, W. Ma, and H. Zhang. 2009. "Remote Sensing Evaluation of Urban Heat Island and Its Spatial Pattern of the Shanghai Metropolitan Area, China." *Ecological Complexity* 6: 413–420.

Li, J., and H. M. Zhao. 2003. "Detecting Urban Land-Use and Land-Cover Changes in Mississauga Using Landsat TM Images." *Journal of Environmental Informatics* 2: 38–47.
Liang, S. 2001. "An Optimization Algorithm for Separating Land Surface Temperature and Emissivity from Multispectral Thermal Infrared Imagery." *IEEE Transactions on Geoscience and Remote Sensing* 39: 264–265.
Liu, H., and Q. Weng. 2008. "Seasonal Variations in the Relationship Between Landscape Pattern and Land Surface Temperature in Indianapolis, USA." *Environmental Monitoring and Assessment* 144: 199–219.
Lu, D., and Q. Weng. 2005. "Urban Classification Using Full Spectral Information of Landsat ETM+ Imagery in Marion County, Indiana." *Photogrammetric Engineering & Remote Sensing* 71: 1275–1284.
Memon, R. A., D. Y. C. Leung, and C.-H. Liu. 2009. "An Investigation of Urban Heat Island Intensity (UHII) as an Indicator of Urban Heating." *Atmospheric Research* 94: 491–500.
Nichol, J. E., W. Y. Fung, K. Lam, and M. S. Wong. 2009. "Urban Heat Island Diagnosis Using ASTER Satellite Images and 'in Situ' Air Temperature." *Atmospheric Research* 94: 276–284.
Owen, T. W., T. N. Carlson, and R. R. Gilies. 1998. "An Assessment of Satellite Remotely-Sensed Land Cover Parameters in Quantitatively Describing the Climatic Effect of Urbanization." *International Journal of Remote Sensing* 19: 1663–1681.
Qian, L. X., H. S. Cui, and J. Chang. 2006. "Impacts of Land Use and Cover Change on Land Surface Temperature in the Zhujiang Delta." *Pedosphere* 16: 681–689.
Rottenborn, S. C. 1999. "Predicting the Impacts of Urbanization on Riparian Bird Communities." *Biological Conservation* 88: 289–299.
Sobrino, J. A., J. C. Jimenez-Munoz, and L. Paolini. 2004. "Land Surface Temperature Retrieval from Landsat TM 5." *Remote Sensing of Environment* 90: 434–440.
Srivastava, P. K., T. J. Majumdar, and A. K. Bhattacharya. 2009. "Surface Temperature Estimation in Singhbhum Shear Zone of India Using Landsat-7 ETM+ Thermal Infrared Data." *Advances in Space Research* 43: 1563–1574.
Stathopoulou, M., and C. Cartalis. 2007. "Daytime Urban Heat Islands from Landsat ETM+ and Corine Land Cover Data: An Application to Major Cities in Greece." *Solar Energy* 81: 358–368.
Streutker, D. R. 2003. "Satellite-Measured Growth of the Urban Heat Island of Houston, Texas." *Remote Sensing of Environment* 85: 282–289.
Umamaheshwaran, R., and Q. Weng. 2009. "Urban Heat Island Monitoring and Analysis Using a Non-Parametric Model: A Case Study of Indianapolis." *ISPRS Journal of Photogrammetry and Remote Sensing* 64: 86–96.
Xiao, H., and Q. Weng. 2007. "The Impact of Land Use and Land Cover Changes on Land Surface Temperature in a Karst Area of China." *Journal of Environmental Management* 85: 245–257.
Zhang, J., and Y. Wang. 2008. "Study of the Relationships Between the Spatial Extent of Surface Urban Heat Islands and Urban Characteristic Factors Based on Landsat ETM+ Data." *Sensors* 8: 7453–7468.